



**HAL**  
open science

## Springtime transitions of NO<sub>2</sub>, CO, and O<sub>3</sub> over North America: Model evaluation and analysis

Yunsoo Choi, Yuhang Wang, Tao Zeng, Derek Cunnold, Eun-Su Yang, Randall Martin, Kelly Chance, Valérie Thouret, Eric Edgerton

► **To cite this version:**

Yunsoo Choi, Yuhang Wang, Tao Zeng, Derek Cunnold, Eun-Su Yang, et al.. Springtime transitions of NO<sub>2</sub>, CO, and O<sub>3</sub> over North America: Model evaluation and analysis. *Journal of Geophysical Research*, 2008, 113, pp.D20311. 10.1029/2007JD009632 . hal-00622941

**HAL Id: hal-00622941**

**<https://hal.science/hal-00622941>**

Submitted on 16 Jun 2022

**HAL** is a multi-disciplinary open access archive for the deposit and dissemination of scientific research documents, whether they are published or not. The documents may come from teaching and research institutions in France or abroad, or from public or private research centers.

L'archive ouverte pluridisciplinaire **HAL**, est destinée au dépôt et à la diffusion de documents scientifiques de niveau recherche, publiés ou non, émanant des établissements d'enseignement et de recherche français ou étrangers, des laboratoires publics ou privés.

Copyright

## Springtime transitions of NO<sub>2</sub>, CO, and O<sub>3</sub> over North America: Model evaluation and analysis

Yunsoo Choi,<sup>1,2</sup> Yuhang Wang,<sup>1</sup> Tao Zeng,<sup>1</sup> Derek Cunnold,<sup>1</sup> Eun-Su Yang,<sup>1</sup> Randall Martin,<sup>3,4</sup> Kelly Chance,<sup>4</sup> Valerie Thouret,<sup>5</sup> and Eric Edgerton<sup>6</sup>

Received 21 November 2007; revised 18 March 2008; accepted 29 July 2008; published 24 October 2008.

[1] Surface observations from AIRNow and Southeastern Aerosol Research and Characterization Study networks, aircraft observations from the Measurement of Ozone and Water Vapor by Airbus In-Service Aircraft program, ozonesondes, and remote sensing measurements from Global Ozone Mapping Experiment, Total Ozone Mapping Spectrometer (TOMS), and Stratospheric Aerosol and Gas Experiment (SAGE) II for February–May 2000 over North America are used to characterize the springtime transitions of O<sub>3</sub> and its precursors. These measurements provide a comprehensive data set to evaluate the performance of the 3-D Regional Chemical Transport Model (REAM). The model is then applied to analyze the key factors affecting the springtime transitions of trace gas concentrations and export. The global GEOS-CHEM model is used to provide chemical initial and boundary conditions. Generally, the model results are in good agreement with the observations in the troposphere except for a low bias of upper tropospheric O<sub>3</sub>; the bias decreases toward the summer and lower latitudes. The rate of observed surface O<sub>3</sub> increase in spring is simulated well by REAM. It is overestimated by GEOS-CHEM over the eastern United States. A key factor driving the model difference is daytime mixing depth. A shallow boundary layer in REAM leads to more efficient removal of radicals and hence slower activation of photochemistry in spring, when the primary radical source is relatively small. Comparison of top-down estimates of fossil fuel NO<sub>x</sub> emissions between REAM and GEOS-CHEM shows model dependence. The associated uncertainty is up to 20% on a monthly basis. Averaging over a season reduces this uncertainty. While tropospheric column NO<sub>2</sub> decreases over the continent, it increases over the western North Atlantic due to lightning NO<sub>x</sub> production. Consequently, the REAM model simulates significant increases of tropospheric O<sub>3</sub> over the region as indicated by column data derived from TOMS-SAGE II. Lightning impact is also evident in model-simulated NO<sub>x</sub> exports.

**Citation:** Choi, Y., Y. Wang, T. Zeng, D. Cunnold, E.-S. Yang, R. Martin, K. Chance, V. Thouret, and E. Edgerton (2008), Springtime transitions of NO<sub>2</sub>, CO, and O<sub>3</sub> over North America: Model evaluation and analysis, *J. Geophys. Res.*, *113*, D20311, doi:10.1029/2007JD009632.

### 1. Introduction

[2] Ozone (O<sub>3</sub>), carbon monoxide (CO), and nitrogen oxides (NO<sub>x</sub> = NO + NO<sub>2</sub>), which are regulated under the National Ambient Air Quality Standards, are among the six

criterion pollutants that adversely affect human health and biological ecosystems [*National Research Council*, 1991]. Ozone is a major precursor of the hydroxyl radical (OH), which plays a key role in oxidation chemistry in the troposphere. It is also a greenhouse gas, particularly in the upper troposphere. NO<sub>x</sub> and CO are major O<sub>3</sub> precursors produced during combustion. NO<sub>x</sub> is also emitted from soils and lightning, and CO can be produced during the oxidation of anthropogenic and biogenic hydrocarbons.

[3] Springtime is a unique period to understand the behaviors of O<sub>3</sub> and its precursors over North America because of the rapid changes in the photochemical and dynamical conditions of the atmosphere. These changes are driven primarily by increasing solar insolation. The solar input energizes photochemical and meteorological processes directly by increasing radical sources through photolysis and the surface sensible and latent heat fluxes, respectively.

<sup>1</sup>School of Earth and Atmospheric Sciences, Georgia Institute of Technology, Atlanta, Georgia, USA.

<sup>2</sup>Now at Jet Propulsion Laboratory, California Institute of Technology, Pasadena, California, USA.

<sup>3</sup>Department of Physics and Atmospheric Science, Dalhousie University, Halifax, Nova Scotia, Canada.

<sup>4</sup>Harvard-Smithsonian Center for Astrophysics, Cambridge, Massachusetts, USA.

<sup>5</sup>Laboratoire d'Aerologie, CNRS, Toulouse, France.

<sup>6</sup>Atmospheric Research and Analysis, Inc., Durham, North Carolina, USA.

[4] Meteorological changes are a powerful force that leads to changes in chemical processes. First, increasing water vapor due to warmer temperature increases the primary radical source through OH production from the reaction of  $O(^1D)$  and  $H_2O$ , which results in more active photochemistry [e.g., Wang *et al.*, 2003a; Kondo *et al.*, 2004]. Second, the abundance of water vapor and surface heating increase convection and lightning [Rind, 1998; Price, 2000], which is a large source of  $NO_x$  in the free troposphere [e.g., Price *et al.*, 1997]. Third, warmer surface temperature and precipitation increase  $NO_x$  emissions from soils [e.g., Yienger and Levy, 1995]. One key atmospheric chemical species affected by all these processes is tropospheric  $O_3$ .

[5] The Tropospheric Ozone Production about the Spring Equinox (TOPSE) experiment of 2000 was designed to measure tropospheric chemical changes during the spring transition period [Atlas *et al.*, 2003]. The experiment took place from February to May 2000 over North America covering the region from Colorado to north of Thule, Greenland. These measurements were taken over remote regions at middle and high latitudes; in situ photochemistry [e.g., Cantrell *et al.*, 2003; Wang *et al.*, 2003a] and large-scale transport of  $O_3$  and its precursors to the measurement regions [e.g., Emmons *et al.*, 2003; Lamarque and Hess, 2003; Wang *et al.*, 2003b; Allen *et al.*, 2003; Y. Wang *et al.*, 2006] are among the foci of previous TOPSE-related tropospheric chemistry analyses.

[6] In this work, we explore the other aspects of tropospheric chemical changes during the spring transition periods, not covered by previous TOPSE-related analyses, using the rich data sets of in situ and satellite measurements available during the same time period over North America. In the process, we evaluate the Regional Chemical Transport Model (REAM). Certain aspects of this model have been evaluated in our previous applications of this model to analyze tropospheric chemistry and transport over the polar regions [Zeng *et al.*, 2003, 2006; Wang *et al.*, 2007] and North America [Choi *et al.*, 2005; Jing *et al.*, 2006; Y. Wang *et al.*, 2006; Guillas *et al.*, 2008]. However, those evaluations lacked breadth because of the nature of the previous analyses. This is the first time that the evaluations of REAM model results with an extensive array of the observations are presented. For comparison purposes, selected results from the global GEOS-CHEM model are used to illustrate key factors contributing to the observed features of springtime transitions of chemicals.

[7] The springtime chemical changes provide a critical test for the simulation capability of REAM. The quality of the emission inventories strongly affects the model simulations of air quality. Emissions of  $NO_x$ , in particular, are important for near-surface  $O_3$  simulations. Satellite observations provide powerful constraints on surface  $NO_x$  emissions [e.g., Martin *et al.*, 2003]. We evaluate the model  $NO_x$  emission inventory using satellite  $NO_2$  measurements first. We further investigate the springtime transitions of different  $NO_x$  sources. Second, we explore the changes of near-surface  $O_3$ , CO, and  $NO_x$  concentrations during spring. Surface air quality changes are characterized from the observations of two monitoring networks, AIRNow by the U.S. Environmental Protection Agency (EPA) and the Southeastern Aerosol Research and Characterization Study

(SEARCH). Third, we study the springtime changes of free-tropospheric  $O_3$  as characterized by in situ measurements from the Measurement of Ozone and Water Vapor by Airbus In-Service Aircraft (MOZAIC) program and ozone-sondes, and tropospheric column  $O_3$  derived from the Total Ozone Mapping Spectrometer (TOMS) and the Stratospheric Aerosol and Gas Experiment (SAGE) II. Last, using the results of the REAM model, we examine the springtime exports of  $O_3$  and its precursors from North America [e.g., Horowitz *et al.*, 1998; Liang *et al.*, 1998; Park *et al.*, 2004].

[8] We first describe the in situ and satellite measurements. The regional REAM and global GEOS-CHEM models are then described. After that, we examine the specific aspects of the springtime transitions of  $NO_x$ , CO, and  $O_3$ . Last, we investigate the import and exports of these trace gases in spring. Conclusions are given in the end. In the appendix, we describe briefly the comparison of REAM simulations to observed column CO by the Measurement of Pollution in the Troposphere (MOPITT) instrument.

## 2. Measurements

### 2.1. In Situ Measurements

#### 2.1.1. EPA AIRNow Network

[9] Hourly  $O_3$  concentrations are obtained from the EPA AIRNow data archives. The sites are divided into three categories: urban, suburban, and rural. The 291 rural sites are used since they are more representative of the region than urban sites. The detection limit value for  $O_3$  was 5 ppbv. We focus on the afternoon (1300 to 1700 LT) when surface observations are more representative because of strong turbulent mixing in the planetary boundary layer (PBL). The CO and  $NO_x$  measurements are not used because of their high method detection limits of 0.5 ppmv for CO and 5 ppbv for  $NO_x$  (J. Summers, personal communication, 2004). Rural CO and  $NO_x$  measurements are usually below the detection limit values (reported as one-half the detection limit).

#### 2.1.2. SEARCH Network

[10] Hourly  $O_3$ , NO, and CO are measured at eight SEARCH sites: Yorkville in Georgia (YRK, rural), Jefferson Street in Atlanta, Georgia (JST, urban), Centreville in Alabama (CTR, rural), Birmingham in Alabama (BHM, urban), Gulfport in Mississippi (GFP, urban), Oak Grove in Mississippi (OAK, rural), Outlying Landing Field 8 in Florida (OLF, suburban), and Pensacola in Florida (PNS, urban). For our analysis, we use observations from the following rural and suburban sites: YRK (85°W, 34°N), CTR (87°W, 33°N), OAK (89°W, 32°N), and OLF (87°W, 30°N). The detection limits of  $O_3$ , NO, and CO are 1 ppbv, 50 pptv, and 10 ppbv, respectively.

#### 2.1.3. MOZAIC Program

[11] The MOZAIC program was designed to automatically collect  $O_3$  and water vapor data on five commercial Airbus A340 aircraft [Marenco *et al.*, 1998]. For recent updates, see <http://www.aero.obs-mip.fr/mozaic/>. For the ascent and descent portions of the flights, MOZAIC raw data (4-s time resolution) are averaged over 150-m height intervals. The MOZAIC analyzer is the dual-beam UV absorption Model 49–103 from Thermo Environment Instruments [Thouret *et al.*, 1998]. The instruments are laboratory-calibrated before and after flight periods and

laboratory-recalibrated every 12 to 18 months. During flight operation, the instrument is automatically checked for zero and the calibration factor using a built-in O<sub>3</sub> generator.

#### 2.1.4. Ozonesondes

[12] We use ozonesonde data from six midlatitude stations located between 35° and 53°N: Goose Bay (53°N, 50°W), Richland (46°N, 119°W), Trinidad Head (41°N, 124°W), Boulder (40°N, 105°W), Wallops Island (38°N, 75°W), and Huntsville (35°N, 87°W). The electrochemical concentration cell (ECC) sensor is typically used and the accuracy is about ±6% on the ground and −7% to 17% in the middle and upper troposphere [Komhyr *et al.*, 1995]. The ozonesonde data are obtained from the World Ozone and Ultraviolet Data Center (WOUDC).

## 2.2. Satellite Measurements

### 2.2.1. Tropospheric NO<sub>2</sub> Vertical Column From GOME

[13] The Global Ozone Mapping Experiment (GOME) instrument is on board the European Remote Sensing-2 (ERS-2) satellite that passes over the equator at 1030 local time (LT), and its typical horizontal resolution is 40 km (along track) by 320 km (cross track). The retrieval algorithm and air mass factor calculation are described in detail by Chance *et al.* [2000] and Martin *et al.* [2002]. First, the NO<sub>2</sub> slant column is determined by fitting directly backscattered radiance spectra measured by GOME. Then the stratospheric column determined from the NO<sub>2</sub> column over the central Pacific [Martin *et al.*, 2002] is subtracted from the total column. Finally, the subtracted columns are converted to vertical columns using air mass factors, which are an integral of the product of the shape factor from model-calculated vertical profiles and the sensitivity of backscattered radiance to NO<sub>2</sub>. The radiance perturbation due to the change of NO<sub>2</sub> is calculated from the Linearized Discrete Ordinate Radiative Transfer (LIDORT) model [Spurr *et al.*, 2001], which considers multiple scattering in the atmosphere. Data of cloud optical depth and fraction are from GOME [Kurosui *et al.*, 1999]. The monthly mean fields of aerosol mass concentrations are taken from the Global Ozone Chemistry Aerosol Radiation and Transport (GOCART) model [Chin *et al.*, 2002], which simulates 3-D distributions of sulfate, mineral dust, sea salt, black carbon, and organic carbon. We do not use GOME measurements when cloud cover is >40% [Martin *et al.*, 2002]. The retrieval uncertainties are mostly due to spectral fitting, spectral artifacts related to the diffuser plate, removal of the stratospheric column, and air mass factor calculations [Martin *et al.*, 2002; Choi *et al.*, 2005]. The uncertainties are generally  $0.6\text{--}1.2 \times 10^{15}$  molecules cm<sup>−2</sup> over the ocean and  $1.0\text{--}3.5 \times 10^{15}$  molecules cm<sup>−2</sup> over the continent.

### 2.2.2. Tropospheric O<sub>3</sub> Column From TOMS and SAGE II

[14] TOMS on board the Earth Probe satellite that crosses the equator at 1116 local time measures incident solar radiation and backscattered ultraviolet sunlight. Total atmospheric O<sub>3</sub> columns have a horizontal resolution of  $39 \times 39$  km<sup>2</sup> with a measurement uncertainty of about 5%. SAGE II on board the Earth Radiation Budget Satellite (ERBS) measured the Earth limb extinction via the solar occultation technique during each spacecraft sunrise and sunset. The horizontal and vertical resolutions of SAGE are about  $30 \times$

250 km<sup>2</sup> and 1 km, respectively. Scatterplots of SAGE II (retrieval version 6.2) O<sub>3</sub> versus potential vorticity (PV) on isentropic surfaces are used to produce the O<sub>3</sub> profiles in the stratosphere [Jing *et al.*, 2004], which are coincident in latitude, longitude, and time with TOMS (version 8) total column O<sub>3</sub> measurements. When the TOMS data indicate a reflectivity <20%, tropospheric O<sub>3</sub> columns are inferred by subtracting the SAGE II-based stratospheric from the TOMS columns. The PV values are obtained from the NCEP reanalysis data set, and a value of 3.5 PV units is used to define the location of the tropopause.

[15] By comparisons with the ozonesonde measurements, two previous studies [H.-J. Wang *et al.*, 2002, 2006] indicate that SAGE O<sub>3</sub> has an accuracy of 10% or better down to the tropopause and that the SAGE data are 5% higher than the ozonesonde values at 15–20 km. The PV-mapped SAGE O<sub>3</sub> column estimates between 340 and 800 K isentropic surfaces (~10–30 km) have a 4% error, compared to the ozonesonde observations at 30–60°N. Considering that 90% of total column O<sub>3</sub> resides in the stratosphere, the uncertainty of the derived tropospheric column O<sub>3</sub> is ~40%. The uncertainty is expected to decrease when tropospheric columns are averaged over a period of a month. In our analysis, we focus more on the qualitative aspects of model results in comparison to TOMS-SAGE II tropospheric O<sub>3</sub> columns.

## 3. Model Descriptions

[16] In this work, REAM has a horizontal resolution of 70 km with 23 vertical layers reaching 10 hPa, 20 of which are below 100 hPa. The National Center for Atmospheric Research/Penn State MM5 is used to simulate meteorological fields using four-dimensional data assimilation (FDDA) [Stauffer *et al.*, 1991] based on the National Center for Environmental Prediction reanalysis, surface, and rawinsonde observations. Most of the meteorological variables are archived every 30 min, except those for convection and lightning which are archived every 2.5 min because of the highly variable nature of these processes. The horizontal domain of MM5 has five extra grids on each side of the REAM domain to minimize potential transport anomalies near the boundary. We use the ETA Mellor-Yamada-Janjic (MYJ) 2.5-order closure scheme [Black, 1994] for turbulence calculations. Regional simulations are spun up in the last week of January 2000.

[17] The photochemical, dry, and wet deposition modules of REAM are adopted from the GEOS-CHEM model [Bey *et al.*, 2001]. The altitude-dependent cloud optical depth is calculated using MM5 liquid water content [Stephens *et al.*, 1978]. The UV surface albedo distribution, for photolysis rate calculations, is obtained from TOMS observations [Herman and Celarier, 1997]. The transport scheme is from Walcek [2000]. The convective scheme by Grell [1993] is implemented to be consistent with the meteorological model; subgrid-scale updraft and downdraft processes and large-scale subsidence are considered. The top and bottom layers of shallow convection are determined by MM5 simulations; the cloud fraction is determined using the scheme described by Geleyn [1981].

[18] Emission inventories for combustion and industrial sources are taken from GEOS-CHEM [Bey *et al.*, 2001],

except the fossil fuel  $\text{NO}_x$  and CO emission inventories over the United States, which are taken from the 1999 U.S. Environmental Protection Agency National Emission Inventory. These values are scaled with the national total emissions of 2000 [U. S. Environmental Protection Agency, 2003]. Emission algorithms for vegetation and soils are adopted from GEOS-CHEM, although meteorological inputs are from MM5. Parameterizations of  $\text{NO}_x$  from lightning as functions of convective mass flux and convective available potential energy are the same as described by Choi *et al.* [2005].

[19] Spring 2000 GEOS-CHEM model simulations provide initial and boundary conditions for trace gases. GEOS-CHEM (version 7.2) is driven by GEOS assimilated meteorological fields (GEOS-3) for 2000. The horizontal resolution of GEOS-CHEM is  $2^\circ$  latitude by  $2.5^\circ$  longitude. Detailed algorithms for photochemistry, dry and wet deposition, and emissions, many of which are adopted in REAM as discussed above, are described by Bey *et al.* [2001]. Algorithms of  $\text{NO}_x$  emissions from lightning based on cloud top height by Price and Rind [1994] and from soils by Yienger and Levy [1995] were adapted by Wang *et al.* [1998].

#### 4. Surface Emissions of Fossil Fuel $\text{NO}_x$

[20] In situ observations of  $\text{NO}_x$  from the EPA surface network do not provide constraints on surface  $\text{NO}_x$  emissions because of instrument issues (section 2.1). What is available to constrain this important  $\text{O}_3$  precursor is column  $\text{NO}_2$  measurements by satellites such as GOME [e.g., Martin *et al.*, 2003]. Because satellite measurements are integrated over the atmospheric column, retrievals are more complex than in situ measurements. We first examine the dependence of  $\text{NO}_2$  retrievals on the a priori model profiles. We then characterize the observed tropospheric vertical column  $\text{NO}_2$  and the factors contributing the observed seasonal change. Last, we apply the inversion method to examine the quantitative constraints on surface  $\text{NO}_x$  emissions.

##### 4.1. Dependence of GOME $\text{NO}_2$ Retrievals on the A Priori Profiles

[21] The retrieval process is described in section 2.2. To obtain the tropospheric vertical columns, model profiles of  $\text{NO}_2$  are used to calculate the air mass factor. As a result, some model dependence of the retrieval is therefore convoluted in the retrieved vertical columns. As will be discussed in the next section, REAM and GEOS-CHEM models simulate different vertical profiles of tropospheric  $\text{NO}_2$  (to be shown in Figure 6). We therefore compute the air mass factors separately from these two model results as a way of examining the sensitivity of GOME retrievals to the simulated  $\text{NO}_2$  vertical profiles. Figure 1 shows good agreement between GOME  $\text{NO}_2$  column retrievals using the REAM and GEOS-CHEM profiles between February and May 2000. The spatial correlation coefficient between the two models is  $>0.99$ . The monthly mean  $\text{NO}_2$  columns of the retrievals using REAM profiles are higher by 6.1, 12.0, 5.5, and 0.4% from February to May than those using GEOS-CHEM profiles. Generally, a value of 15% is estimated as the  $\text{NO}_2$ -profile associated retrieval uncertainty

[Martin *et al.*, 2002], which encompasses the range of model derived difference found here.

##### 4.2. Characterizations of Tropospheric Column $\text{NO}_2$

[22] GOME derived tropospheric  $\text{NO}_2$  columns in Figure 1 shows a decreasing trend over the continental region, particularly over high emissions regions in the Northeast and Midwest of the United States. In contrast, there is a clear increasing trend over the western North Atlantic. Comparing the two model simulations to the retrieved column  $\text{NO}_2$ , the mean biases are within 11%, and the correlations are high ( $R > 0.85$ ). Over the continent, the two models show similar trends as observed. The decreasing trend simulated in the model is driven by more active photochemistry as spring progresses toward summer. As a result, more  $\text{NO}_2$  is removed by the reaction of OH and  $\text{NO}_2$ . Owing to its coarse spatial resolution, the GEOS-CHEM model fails to capture high  $\text{NO}_2$  columns ( $>5 \times 10^{15}$  molecules  $\text{cm}^{-2}$ ) in California, which are shown in REAM results. In April and May, both models slightly underestimate  $\text{NO}_2$  columns in the western United States probably due to underestimated soil  $\text{NO}_x$  emissions [e.g., Martin *et al.*, 2003; Bertram *et al.*, 2005]. While REAM tends to slightly overestimate GOME  $\text{NO}_2$  columns in May partly due to larger lightning  $\text{NO}_x$  productions, GEOS-CHEM tends to underestimate.

[23] The large increase of column  $\text{NO}_2$  over the western North Atlantic, despite increasing photochemical removal as the season progresses is captured by REAM. In comparison, no significant changes are shown in GEOS-CHEM simulations, leading to underestimates of column  $\text{NO}_2$  in the region. We discuss the contributions of several factors to tropospheric column  $\text{NO}_2$  in section 4.3.

##### 4.3. Contributions of Lightning, Soil Emissions, and Convection to Column $\text{NO}_2$

[24] We compute the contributions of lightning production, convective transport, and soil emissions in the model by comparing the standard REAM simulation against simulations with one of these processes turned off. Figure 2 shows monthly mean column differences between the standard and sensitivity simulations. In February and March, lightning  $\text{NO}_2$  enhancements are typically  $<3.0 \times 10^{14}$  molecules  $\text{cm}^{-2}$ , but in April and May, they increase to  $0.5\text{--}2.0 \times 10^{15}$  molecules  $\text{cm}^{-2}$  over the southern United States, the Gulf of Mexico, and the western North Atlantic. Typical monthly mean uncertainties for GOME retrievals are  $2\text{--}9 \times 10^{14}$  molecules  $\text{cm}^{-2}$  over ocean, which is 20–70% of typical uncertainties over the continent. Large enhancements from lightning and soil emissions simulated in May are larger than the retrieval errors on a monthly mean basis.

[25] The lightning and soil emission contributions over land increase to 10 and 7% of tropospheric column  $\text{NO}_2$ , respectively, in May (from 0.7 and 1.3% in February). The estimated contribution of lightning is larger than that of soil emissions, except in February. The springtime increase of tropospheric column  $\text{NO}_2$  over the western North Atlantic is driven by lightning  $\text{NO}_x$  emissions in the REAM simulations. The fractional contribution to  $\text{NO}_2$  columns over this region by lightning increases from 5% in February to 32% in May. The increasing trend is not simulated by GEOS-

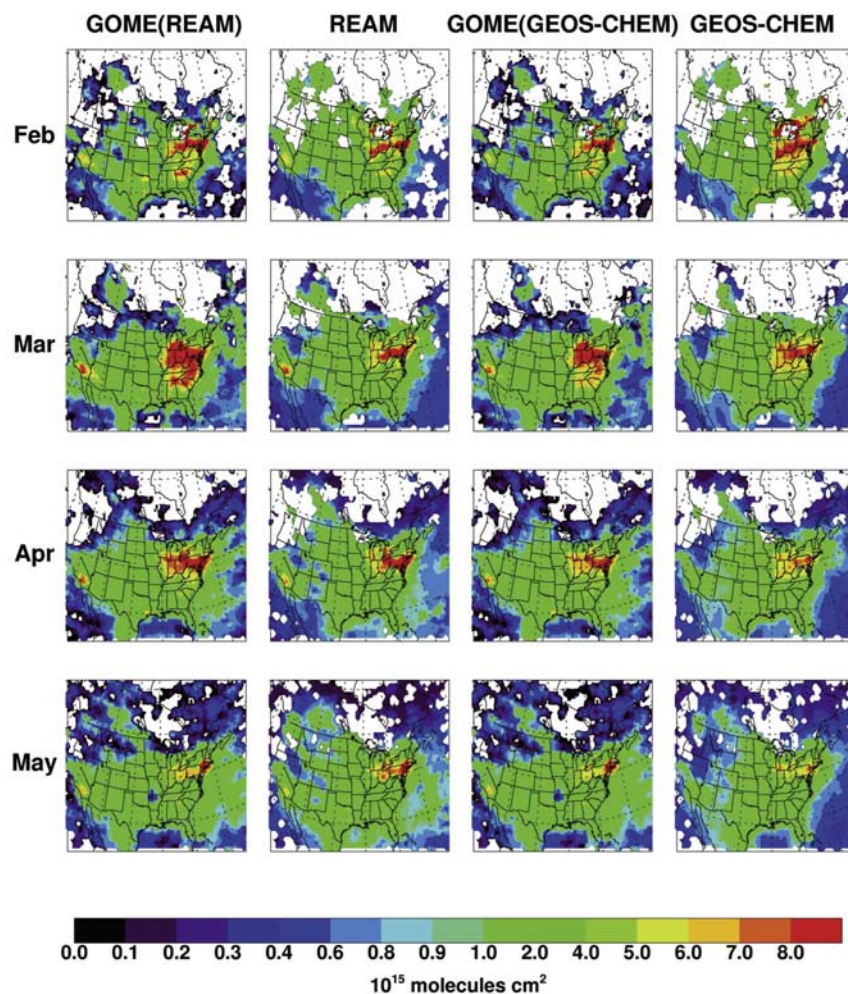


**Figure 1.** Monthly mean tropospheric NO<sub>2</sub> vertical columns during February–May 2000 from Global Ozone Mapping Experiment (GOME) retrievals using the Regional Chemical Transport Model (REAM)-derived shape factor (first column), the REAM model (second column), GOME retrievals using the GEOS-CHEM-derived shape factor (third column), and the GEOS-CHEM model (last column). Only measurements with cloud fraction  $\leq 40\%$  are used. The text provides the description of retrieval process. The model results are obtained by averaging NO<sub>2</sub> data during the satellite overpass time period (1000–1100 LT).

CHEM because the algorithm by *Price and Rind* [1994] gives very low flash rates over the ocean.

#### 4.4. Top-Down Constraints on Fossil Fuel NO<sub>x</sub> Emissions

[26] Optimized NO<sub>x</sub> emissions are estimated by combining top-down NO<sub>x</sub> emission estimates from satellite measurements with a priori bottom-up emissions, weighted by relative errors for the two estimates [*Martin et al.*, 2003]. Both REAM and GEOS-CHEM use the same EPA 1999 NEI inventory for surface fossil fuel NO<sub>x</sub> emissions in the United States as the a priori. One implicit assumption in the method by *Martin et al.* [2003] that we use here is that fossil fuel, soil, and lightning NO<sub>x</sub> emissions are scaled by the same top-down to a priori factor. From February to April, the contributions of soil and lightning emissions to NO<sub>2</sub> columns are  $<7\%$  in REAM and GEOS-CHEM. That fraction increases to 13–17% in May. Considering that the a posteriori changes we calculated are  $<15\%$ , the inversion is largely dominated by fossil fuel NO<sub>x</sub>.

[27] The top-down NO<sub>x</sub> fossil fuel emission inventory ( $E_t$ ) is first calculated following *Martin et al.* [2003] by fitting  $E_t$  to a priori bottom-up emission  $E_a$  with the ratio of the retrieved NO<sub>2</sub> column ( $\Omega_r$ ) to the simulated column ( $\Omega_s$ ):

$$E_t = E_a \times \Omega_r / \Omega_s. \quad (1)$$

Monthly a posteriori emissions ( $E$ ) are then calculated by the weighted averages of  $E_a$  and  $E_t$  [*Martin et al.*, 2003]:

$$\ln E = \frac{(\ln E_t)(\ln \varepsilon_a)^2 + (\ln E_a)(\ln \varepsilon_t)^2}{(\ln \varepsilon_a)^2 + (\ln \varepsilon_t)^2} \quad (2)$$

where  $\varepsilon_a$  and  $\varepsilon_t$  are the a priori inventory and top-down emission errors, respectively.

[28] Table 1 shows the monthly a priori, top-down, and a posteriori emissions derived using REAM and GEOS-CHEM results, respectively. The a priori emissions

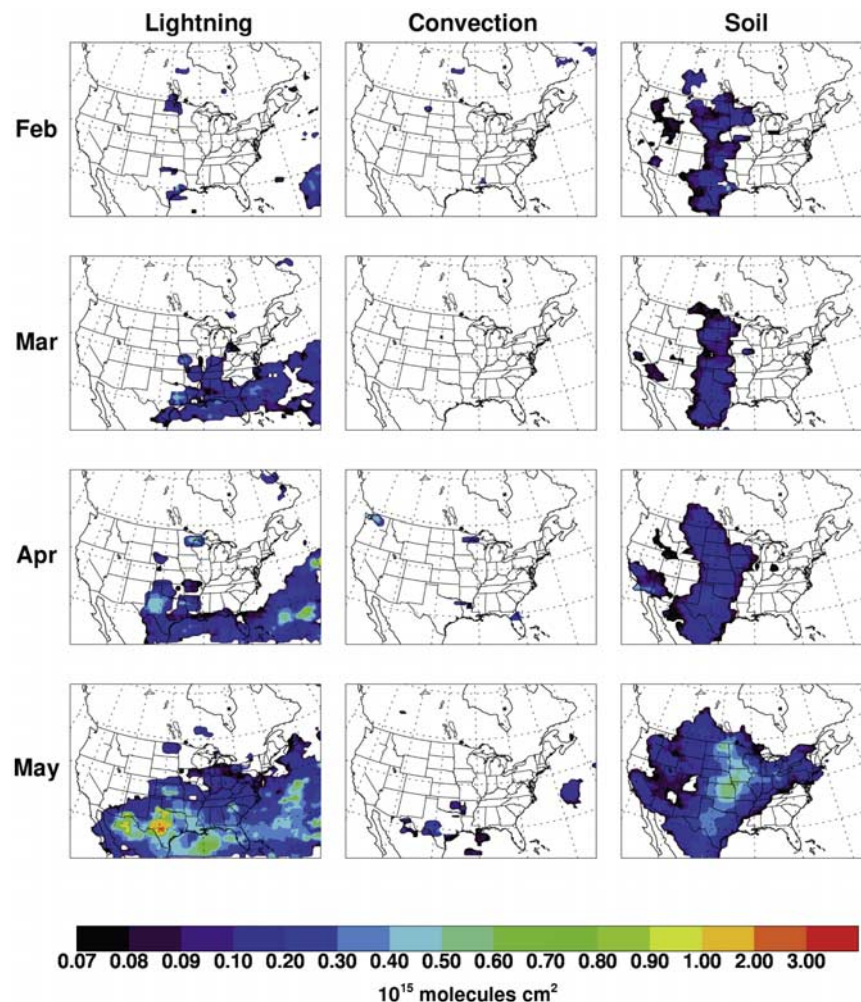


**Figure 2.** Monthly mean contributions of lightning production, convection, and soil emissions to tropospheric NO<sub>2</sub> vertical columns.

from REAM and GEOS-CHEM are almost the same, but the top-down estimates sometimes differ significantly. The top-down emissions derived by REAM are larger by 3% to 16% than those of GEOS-CHEM between February and April and are smaller by 20% than GEOS-CHEM in May. Two sources contribute the variations in the top-down estimates. One is due to the difference in model simulated vertical profiles of NO<sub>2</sub> and hence the calculated air mass factors discussed in section 4.1. The other is the difference in model simulated emission-column relationship used in equation (1). For comparison, the standard deviation of monthly averages from the 4-month average is 16–19% in

the each model, comparable to the difference between the two model estimates for each month. Therefore, time averaging (>1 month) is needed to derive a more robust top-down estimate. On a seasonal basis, the top-down and a posteriori emissions are almost exactly the same as the a priori.

## 5. Spring Transitions of Near-Surface Air Quality

[29] Springtime air quality changes can be characterized by the measurements from the EPA AIRNow monitoring network. To avoid the problems in the reported CO and NO<sub>x</sub>

**Table 1.** Monthly North America (20–62°N) Fossil Fuel NO<sub>x</sub> Emissions<sup>a</sup>

	REAM Derived			GEOS-CHEM Derived		
	A Priori	Top-Down	A Posteriori	A Priori	Top-Down	A Posteriori
February	0.57	0.49	0.52	0.55	0.41	0.47
March	0.61	0.76	0.69	0.61	0.66	0.64
April	0.59	0.66	0.63	0.58	0.64	0.61
May	0.61	0.59	0.60	0.60	0.71	0.66
Average	0.60	0.63	0.61	0.59	0.61	0.60

<sup>a</sup>Emissions are measured in Tg N month<sup>-1</sup>. REAM is Regional Chemical Transport Model.

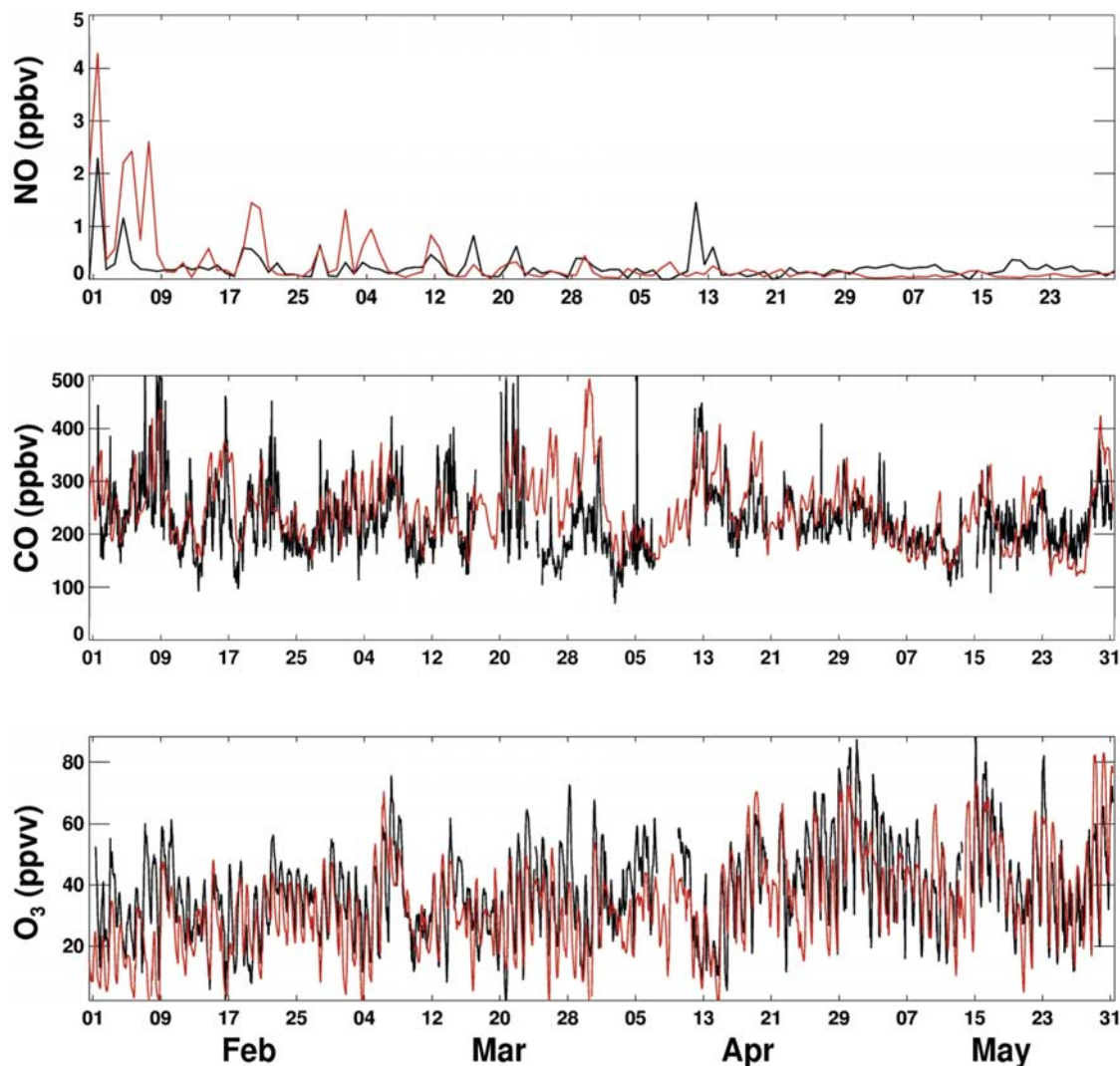


**Figure 3.** Observed and simulated afternoon (1300–1700 LT) average NO and hourly CO and O<sub>3</sub> at the Oak Grove site (89°W, 32°N). The solid black lines represent the Southeastern Aerosol Research and Characterization Study (SEARCH) measurements and red lines represent the REAM results.

measurements from this network (section 2.1), we first make use of the measurements of NO, CO, and O<sub>3</sub> from the SEARCH networks, even though the geographic coverage of the SEARCH data set is limited.

### 5.1. Spring Trends of NO, CO, and O<sub>3</sub> at SEARCH Sites

[30] Inspection of NO, CO, and O<sub>3</sub> concentrations at the four SEARCH rural sites (CTR, OAK, OLF, and YRK, section 2.1) in February–May 2000 reveals that these sites show similar multiday temporal patterns (not shown), which are driven by synoptic-scale meteorological changes over the region. To illustrate the comparison, we show the results at the OAK site in Figure 3. Hourly NO concentrations vary significantly between day and night because of the shallow boundary layer at night. We show only daily 1300–1700 LT values for NO. The temporal variation pattern is not well characterized by NO concentrations even though that periods with elevated NO at all four sites can be found. The model has some capability to capture the NO variations. The multiday synoptic-scale variations are better character-

ized by CO and O<sub>3</sub>, which have longer chemical lifetimes. These variations are simulated by the model.

[31] The correlation coefficients between REAM and SEARCH NO are higher at CTR and OAK sites (0.66 and 0.56, respectively) than OLF and YRK sites (0.40 and 0.23, respectively). The lower correlations at the latter two sites reflect the coastal location of the OLF site and the large influence of power plant emissions at the YRK site. The model resolution is too coarse to simulate properly the influence of power plant plumes. The correlation coefficients for CO are in the range of 0.52–0.63 except the YRK site (0.48). Too much influence from CO emissions in Atlanta is simulated in the model because the proximity of Yorkville to Atlanta (60 km). The correlation coefficients for O<sub>3</sub> are in the range of 0.65–0.69.

[32] The seasonal transitions of NO, CO, and O<sub>3</sub> are different. Concentrations of NO decrease, reflecting in part the increasing photochemical loss of NO<sub>x</sub>. The trend is consistent with GOME measurements (Figure 1). The seasonal decrease of CO is relatively small during spring.

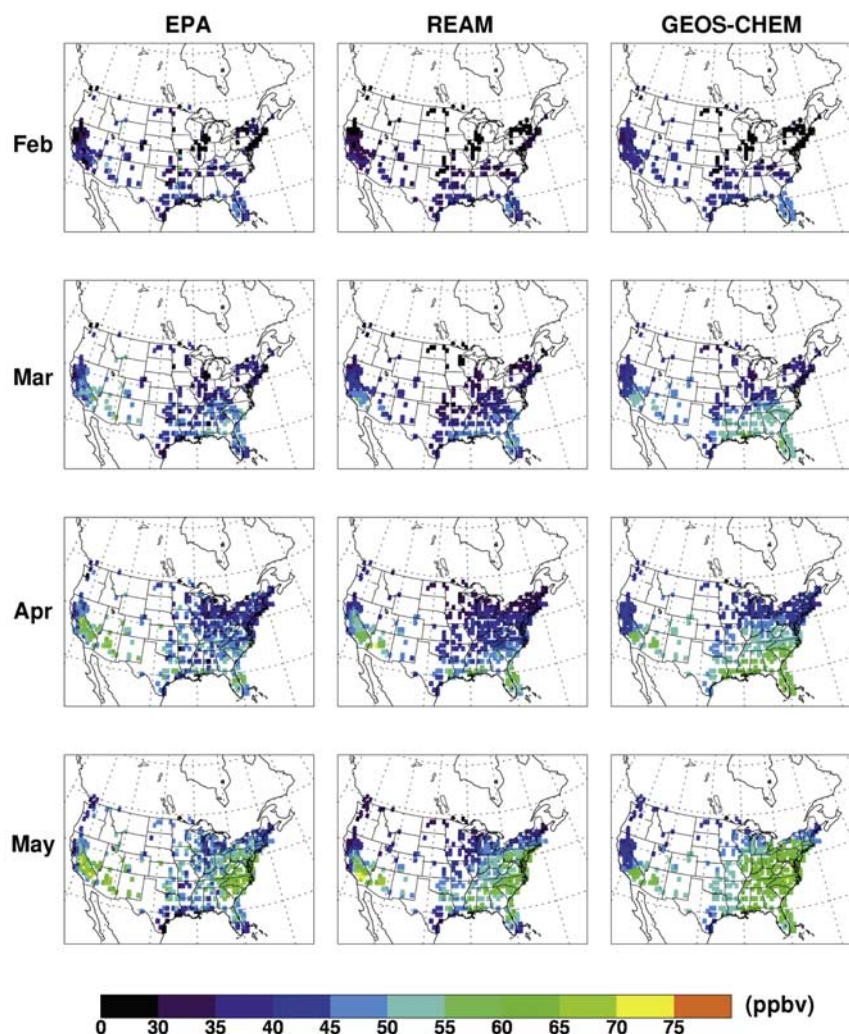


**Figure 4.** Monthly mean afternoon (1300–1700 LT) surface  $O_3$  concentrations (ppbv) over the United States in February–May 2000. Shown are the U. S. Environmental Protection Agency AIRNow observations at rural sites (left column), REAM simulation results (middle column), and GEOS-CHEM simulation results (right column).

Increasing CO loss due to increasing OH oxidation is compensated for by faster CO production from VOC oxidation. Ozone, in comparison, clearly has an increasing trend as photochemistry becomes more active. These trends are simulated well by REAM. We also compared GEOS-CHEM simulations with these surface observations (not shown). One large difference between REAM and GEOS-CHEM is that GEOS-CHEM tends to overestimate surface  $O_3$  concentrations in April and May. We look at this issue using the measurements from the AIRNow network, which has good spatial coverage over the contiguous United States.

## 5.2. Surface $O_3$ Increase in AIRNow Measurements

[33] Monthly mean afternoon (1300–1700 LT)  $O_3$  concentrations measured by the EPA AIRNow surface sites are compared with REAM and the GEOS-CHEM simulations from February to May (Figure 4). High  $O_3$  peaks are captured by REAM to within 10 ppbv. The correlation coefficients of the REAM and GEOS-CHEM results with the measurements are in the range of 0.56–0.65 and 0.44–

0.68, respectively. The correlations between the GEOS-CHEM and AIRNow observations decrease as the season progresses toward summer while the opposite is true for REAM.

[34] As the season progresses toward summer, increasing solar influx and water vapor activates photochemistry [e.g., Wang *et al.*, 2003a]. Both REAM and GEOS-CHEM simulate the resulting increase in surface  $O_3$ . The rates of photochemical activation and surface  $O_3$  increases are better simulated in REAM than in GEOS-CHEM. The global model simulates higher  $O_3$  concentrations over the eastern United States in April and May than AIRNow observations. Inspections of the model difference between REAM and GEOS-CHEM reveal that a major contributing factor is the differences in the boundary layer mixing depth used in the models.

## 5.3. Daytime Mixing Depth and Surface $O_3$

[35] It was known that mixing depth of the boundary layer affects surface  $O_3$  concentrations [e.g., Holzworth, 1964, 1967]. From February to May, both MM5 and GEOS-

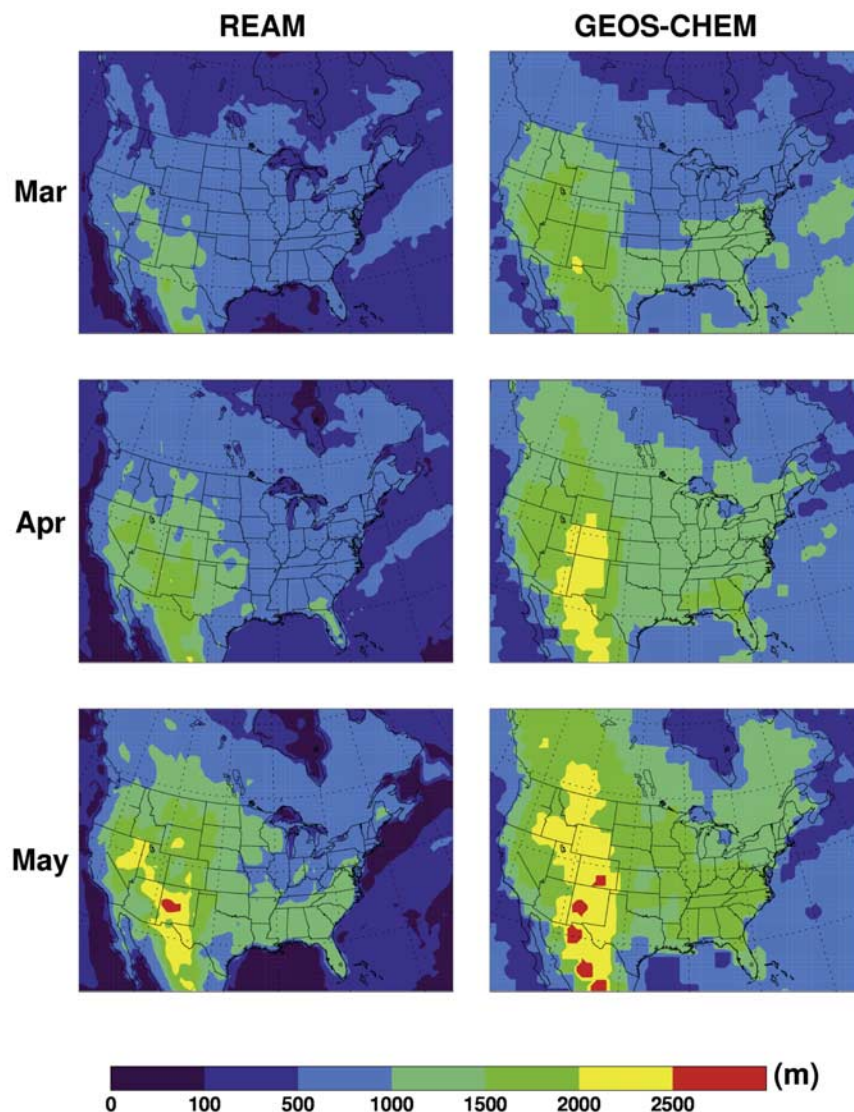


**Figure 5.** Average afternoon (1200–1600 LT) mixing depths over North America in March–May 2000. The data used in REAM (left column) are simulated by MM5, and those used in GEOS-CHEM (right column) are simulated by GEOS-3.

3 predict increasing boundary layer mixing depth as solar insolation increases (Figure 5). However, MM5 predicted mixing depths (used in REAM) are in general lower than GEOS-3 predictions (used in GOES-CHEM). The difference is particularly large over the eastern United States, where the difference is up to a factor of 2. Unfortunately, routine meteorological observations do not provide useful information to evaluate model simulated afternoon mixing depth.

[36] The shallower mixing depth in REAM results in stronger boundary layer vertical gradients and higher surface concentrations of CO and NO<sub>x</sub> but lower concentrations of O<sub>3</sub> than GEOS-CHEM over the eastern United States (Figure 6). The effect of boundary layer mixing is best demonstrated by CO distributions since its photochemical source is relatively small compared to emissions and its lifetime is long. Below 900 hPa, REAM simulates higher concentrations than GEOS-CHEM. The opposite is true

between 700 and 850 hPa, reflecting more efficient mixing in GEOS-CHEM. From March to May, the difference of CO near the surface REAM and GEOS-CHEM increases, reflecting a faster mixing depth increase in GEOS-CHEM than REAM. Similar characteristics are found for NO<sub>x</sub> and O<sub>3</sub>. Surface CO and NO<sub>x</sub> are larger by ~50 ppbv and ~1 ppbv, respectively, in the REAM results. In contrast, REAM surface O<sub>3</sub> mixing ratios are lower by 5–10 ppbv. REAM simulated increase of NO<sub>x</sub> concentrations in the upper troposphere, particularly in May, is due to lightning NO<sub>x</sub> production.

[37] During spring, the radical source, which is largely driven by photon flux and water vapor [e.g., Wang *et al.*, 2003a], is limited. High concentrations of NO<sub>x</sub> decrease photochemical activity because of increasing radical loss through the reaction of OH and NO<sub>2</sub>. Thus, less active mixing in REAM results in lower surface O<sub>3</sub> production and concentrations than GEOS-CHEM during spring, lead-

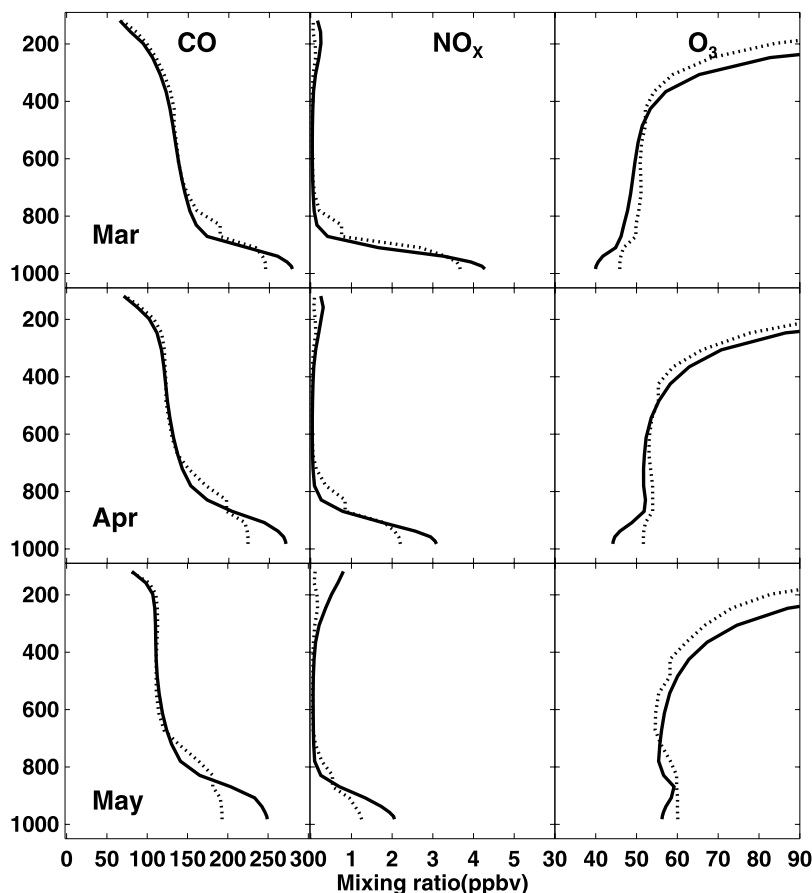


**Figure 6.** Comparisons of monthly averaged afternoon (1200–1600 LT) vertical profiles of CO, NO<sub>x</sub>, and O<sub>3</sub> concentrations between REAM and GEOS-CHEM models. The profile is averaged over the continental region of 75–90°W and 30–42°N. The solid lines represent the REAM simulations, and the dotted lines represent the GEOS-CHEM simulations.

ing to better agreement with AIRNow surface measurements (Figure 4).

## 6. Free-Tropospheric O<sub>3</sub> in Spring

### 6.1. In Situ O<sub>3</sub> Measurements

[38] We first examine in Figure 7a the vertical O<sub>3</sub> profiles from ozonesondes and MOZIAC program during spring. MOZIAC profiles are taken during takeoff and landing from cities including Toronto, New York City, Chicago, Washington, D. C., Atlanta, Houston, and Dallas. Most of the data are over the eastern United States because the measurements were made on commercial flights between the United States and Europe. Model results are in good agreement with the measurements in the lower and middle troposphere, except for a low bias of 10 ppbv at Wallops Island. The site is located at a baroclinic zone with large O<sub>3</sub> gradients [Thouret *et al.*, 2006], making it more difficult to simulate in the model. The boundary layer O<sub>3</sub> trend in spring was discussed in section 5. We investigate the seasonal O<sub>3</sub> trend in the free troposphere (400–800 hPa.) in Figure 7b Ozonesonde and MOZIAC measurements show an increase of ~10 ppbv from February to May. This magnitude of increase is captured well by REAM, although REAM monthly mean mixing ratios are lower than the measurements by ~3 ppbv.

[39] In the upper troposphere, however, the REAM model has a clear tendency to underestimate. To illustrate the spatial and temporal distributions, we show in Figure 8 a comparison of MOZIAC measurements with REAM results at 150–250 hPa from February to May. MOZIAC measurements have better data coverage in this region than lower altitudes because it is close to the cruise altitude of aircraft. We filtered out mixing ratios >200 ppbv in the measurements (and model results) to minimize the effects of extreme values.

[40] In general, REAM tends to underestimate O<sub>3</sub> concentration measurements. Thouret *et al.* [2006] found that spring maximum O<sub>3</sub> in the MOZIAC measurements is located in the lower stratosphere, where O<sub>3</sub> concentrations range from 150 to 500 ppbv with a strong vertical gradient near the tropopause region. The upper tropospheric O<sub>3</sub> simulations in REAM are strongly affected by the specified upper boundary conditions at 100 hPa from GEOS-CHEM, which exhibits difficulties in simulating the sharp O<sub>3</sub> gradient across the tropopause [Bey *et al.*, 2001]. REAM results in the upper troposphere improve toward May as tropospheric photochemical production contributes more to upper tropospheric ozone. In the same vein, Figure 7a shows that model low bias improves significantly as we

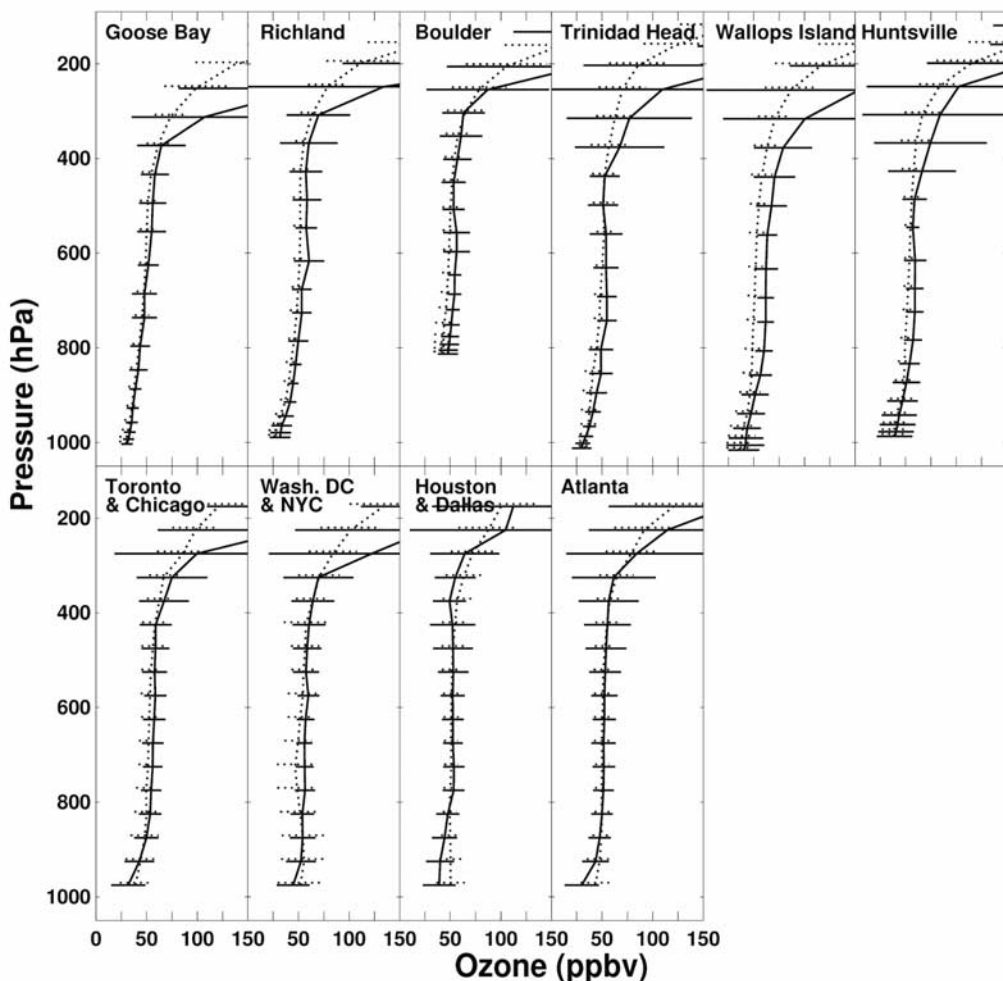


**Figure 7a.** a. Observed and simulated mean  $O_3$  profiles for February–May 2000, showing the observations from (top) ozonesondes and (bottom) Measurement of Ozone and Water Vapor by Airbus In-Service Aircraft (MOZAIC) program in solid lines. Horizontal bars show standard deviations. Dotted lines show corresponding REAM results. The ozonesonde sites include Goose Bay ( $53^\circ\text{N}$ ,  $60^\circ\text{W}$ ), Richland ( $46^\circ\text{N}$ ,  $119^\circ\text{W}$ ), Boulder ( $40^\circ\text{N}$ ,  $105^\circ\text{W}$ ), Rinidad Head ( $41^\circ\text{N}$ ,  $124^\circ\text{W}$ ), Wallops Island ( $38^\circ\text{N}$ ,  $75^\circ\text{W}$ ), and Huntsville ( $35^\circ\text{N}$ ,  $87^\circ\text{W}$ ). “Wash. DC” denotes Washington, D. C., and “NYC” denotes New York City.

move toward the lower-latitude sites or cities, where photochemical production of ozone is more active.

## 6.2. TOMS-SAGE II Tropospheric Column $O_3$

[41] Ozonesonde and MOZAIC data do not provide enough coverage to allow examination of the spatial distribution of the spring increase of tropospheric ozone. We use the tropospheric column  $O_3$  derived from TOMS and SAGE II measurements (section 2.2) here to qualitatively examine the seasonal transition in tropospheric  $O_3$  columns. Figure 9 compares TOMS-SAGE II tropospheric  $O_3$  column with REAM and GEOS-CHEM results from February to May 2000. The satellite products and the models show a spring-time increase in tropospheric  $O_3$  over North America, even though the absolute amounts of column  $O_3$  derived from TOMS and SAGE II do not agree well with either model. Uncertainties in the derived tropospheric column  $O_3$  (section 2.2) are likely a large contributor to the disagreement. High  $O_3$  columns are clearly shown over the

western North Atlantic in the satellite-derived columns, particularly in May. REAM produces significant enhancements over the region while GEOS-CHEM does not. A sensitivity REAM simulation without lightning  $\text{NO}$  production exhibits much weaker enhancements, suggesting that lightning  $\text{NO}$  production is a large contributor to  $O_3$  enhancements over the western North Atlantic. While simulated lightning  $\text{NO}_x$  enhancements cover a broad region (Figure 1), the resulting  $O_3$  enhancements are mainly in the southern region, where solar insolation is large and photochemistry is active.

## 7. Pollutant Import and Export

### 7.1. Vertical Profiles of Pollutant Fluxes

[42] Fluxes of  $\text{NO}_x$ ,  $\text{NO}_y$ ,  $\text{CO}$ , and  $O_3$  imported to and exported from the troposphere over North America are estimated using REAM (the model boundaries are depicted in Figure 9). Fluxes through the western and eastern

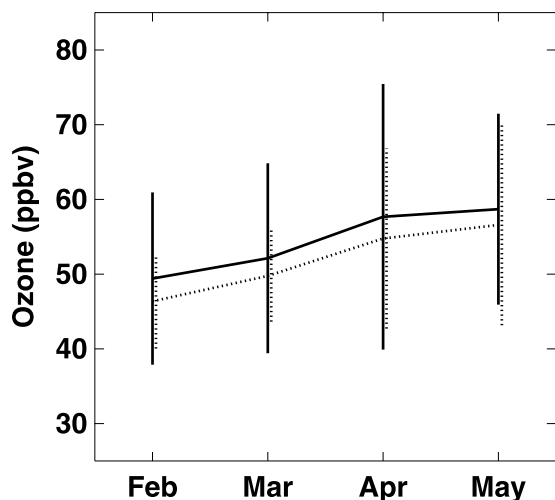


**Figure 7b.** Observed and simulated monthly tropospheric O<sub>3</sub> mixing ratios at 400–800 hPa. The solid lines show means and standard deviations of ozonesonde and MOZAIC measurements. The dotted lines show corresponding REAM results.

boundaries are a factor of 18 larger than through the north and south boundaries. Here, we focus on longitudinal fluxes. Figure 10 shows the vertical profiles of longitudinal import and export fluxes of these pollutants. While the export (in the eastern boundary) of CO decrease, exports of NO<sub>x</sub> and NO<sub>y</sub> show increases. The large increase of NO<sub>x</sub> in the upper troposphere is driven primarily by lightning NO<sub>x</sub> production. For example, simulated NO<sub>x</sub> export fluxes at 12 km increase from  $1.8 \times 10^7$  moles d<sup>-1</sup> to  $4 \times 10^7$  moles d<sup>-1</sup> from February to May. Sensitivity studies (not shown) indicate that lightning production enhances NO<sub>x</sub> and NO<sub>y</sub> exports in the upper troposphere (8–12 km) by 250% and 66%, respectively, in May. Lightning NO<sub>x</sub> is oxidized to longer-lived NO<sub>y</sub> species, which have longer lifetimes. Therefore the vertical gradient of NO<sub>y</sub> export is much less that of NO<sub>x</sub>. The decrease of CO export is associated in part with much longer lifetimes of CO during winter, allowing for the accumulation of CO at middle and high latitudes. As oxidation becomes more active in spring, tropospheric CO concentrations begin to decrease; both export and import fluxes decrease. Ozone export in the upper troposphere is due mainly to transport from the stratosphere over North America in the model.

[43] For comparison with previous studies, we use that by Park *et al.* [2004, hereinafter referred to as PK04] because of the large number of flux values provided. Import fluxes of NO<sub>x</sub> and NO<sub>y</sub> in this study are similar to those from PK04. However, the peak NO<sub>x</sub> and NO<sub>y</sub> exports in May in this study are larger than that from PK04 by a factor of 5 and 38%, respectively. In PK04, less CO was exported than imported above 7 km in June; they suggested that the net import of CO is due to a stronger jet stream over the Pacific than over the Atlantic. A similar feature is also found in May in this study. PK04 shows that less O<sub>3</sub> is exported than imported above 9 km in June. By comparison, we find that O<sub>3</sub> export fluxes are similar to the import fluxes in the upper

troposphere in May, likely due to higher lightning NO<sub>x</sub> production in this study.

## 7.2. Import/Export Fluxes in the Boundary Layer and Export Efficiencies for NO<sub>x</sub> and NO<sub>y</sub>

[44] We chose 2.5 km as the top of the boundary layer as in PK04. Table 2 lists the import and export fluxes. For NO<sub>x</sub> and NO<sub>y</sub>, export fluxes are larger by a factor of >10 than import fluxes. The net export is driven mainly by fossil fuel sources. The imports of O<sub>3</sub> and CO show consistent decreasing trends. Decreasing photochemical lifetimes of these species and weakening westerlies from spring to summer reduce the effects of long-range transport. The exports of O<sub>3</sub> and CO also decrease from February to April. In May, the export of both gases increase because of more active convection in REAM, leading to efficient export into the free troposphere. The net exports estimated in REAM for May are similar to the June estimates by PK04 for NO<sub>x</sub>, NO<sub>y</sub>, and CO. The export of O<sub>3</sub> in REAM (for May) is lower than PK04 (for June). The reasons are likely twofold. First, photochemical production is more active in June than in May. Second, PK04 used meteorological fields from

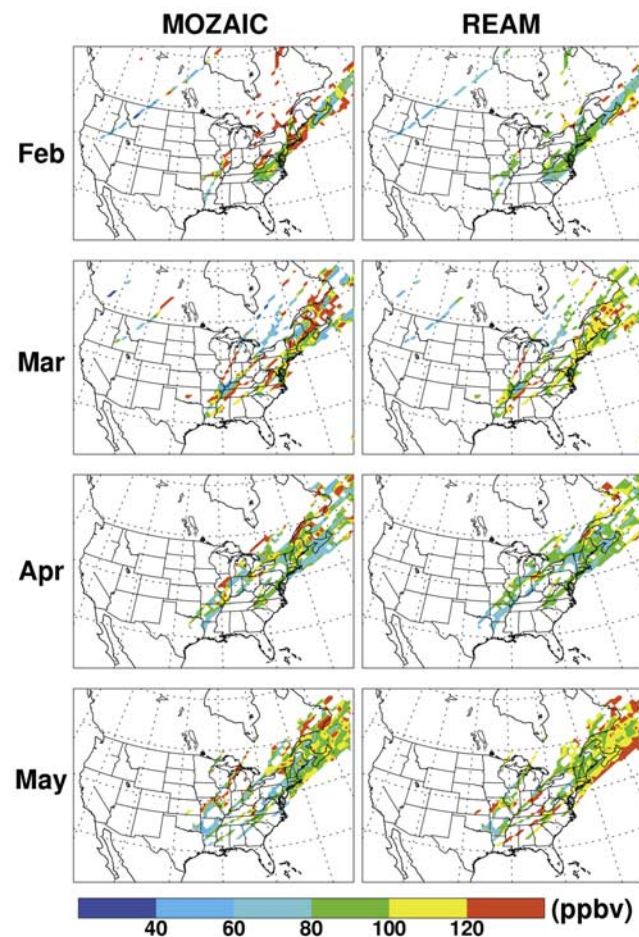


**Figure 8.** Mean O<sub>3</sub> concentration (ppbv) at 150–250 hPa from the MOZAIC measurements during February–May 2000 (left column) and the corresponding REAM results (right column). REAM data are sampled along MOZAIC aircraft tracks. Ozone data >200 ppbv from MOZAIC and REAM are filtered out.

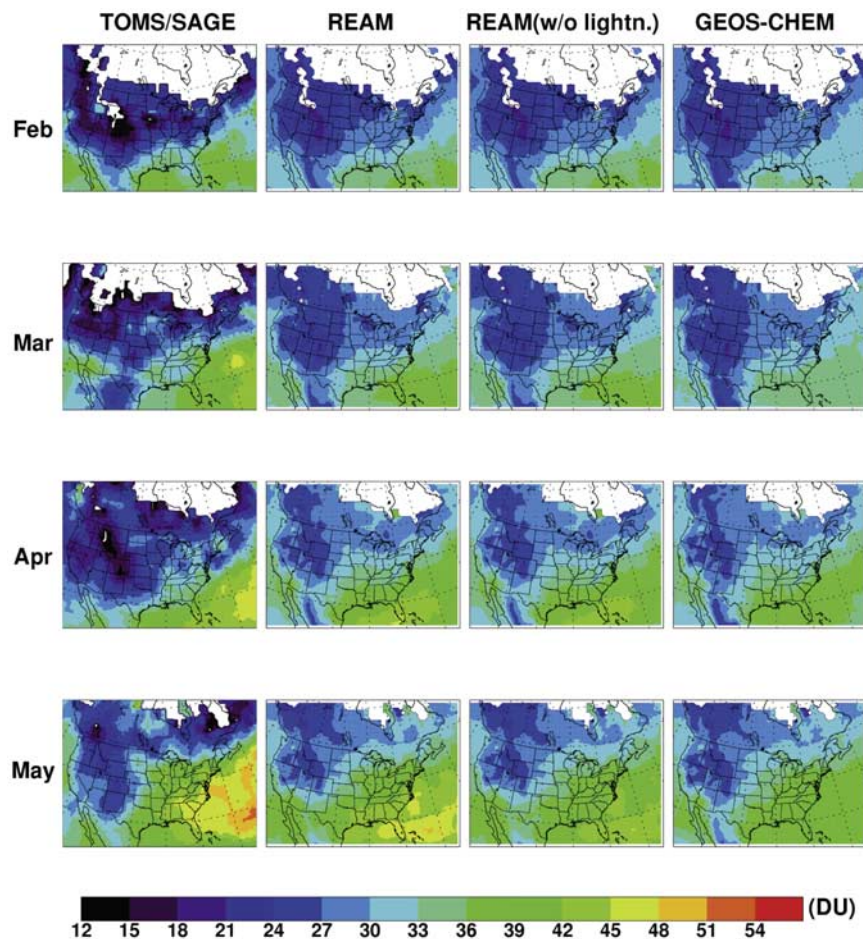


**Figure 9.** Monthly mean tropospheric  $O_3$  columns derived from Total Ozone Mapping Spectrometer total columns and Stratospheric Aerosol and Gas Experiment II stratospheric columns (first column), the REAM standard simulation (second column), the REAM sensitivity simulation without lightning  $NO_x$  production (third column), and the GEOS-CHEM simulation (last column).

GEOS-3 Stretched Grid Data Assimilation System (SG-DAS) [Fox-Rabinovitz *et al.*, 2002], which may also have deeper mixing depths than MM5 simulations used in REAM, resulting in higher  $O_3$  concentrations near the surface, as in the case of GEOS-CHEM (section 5.2).

[45] North American  $NO_x$  emissions (20–62°N) are  $\sim 1.47 \text{ Gmol d}^{-1}$ . About 1.4%, 0.7%, 0.6%, and 0.7% of the emission are exported as  $NO_x$ , and 20%, 12%, 12%, and 14% are exported as  $NO_y$  from the boundary layer from February to May, respectively. The export efficiency of  $NO_x$  decreases as photochemical oxidations becomes more active during spring. However, more active convection toward May increases the export efficiency. As a result, the simulated export efficiencies do not change much from March to May. REAM estimated  $NO_x$  export efficiency in May is comparable to that of PK04 (0.6%), but the efficiency for  $NO_y$  is twice as large as that of PK04 (7%), suggesting that there may be a large difference between the two models in reactive nitrogen speciation.

## 8. Conclusions

[46] The spring transitions of  $O_3$ ,  $NO_x$ , and CO were characterized based on surface, ozonesonde, aircraft, and

satellite measurements over North America from February to May 2000, when rapid photochemical and dynamical changes occur. These observed seasonal changes provide a good testbed to evaluate REAM simulations. The GEOS-CHEM model is used to provide chemical initial and boundary conditions. For illustrations of the effects of key parameters on model simulations, GEOS-CHEM simulations are also used for targeted comparisons with REAM results. The REAM results are generally in good agreement with observations in the troposphere. An exception is the low bias of simulated  $O_3$  concentrations above 350 hPa because the specified upper boundary condition for  $O_3$  (at 100 hPa) is also biased low. The low bias improves toward the summer and toward lower latitudes as tropospheric photochemical production becomes more dominant.

[47] Fossil fuel  $NO_x$  emission inventory is evaluated with GOME measurements. Both REAM and GEOS-CHEM products are used in order to test the model dependence of the top-down emission estimates. The monthly top-down estimates differ between the two models for two reasons. First, the different  $NO_2$  profiles lead to 0–12% difference in monthly air mass factors. Second, model differences lead to a different relationship between surface emissions and column  $NO_2$ . The resulting monthly top-down emission

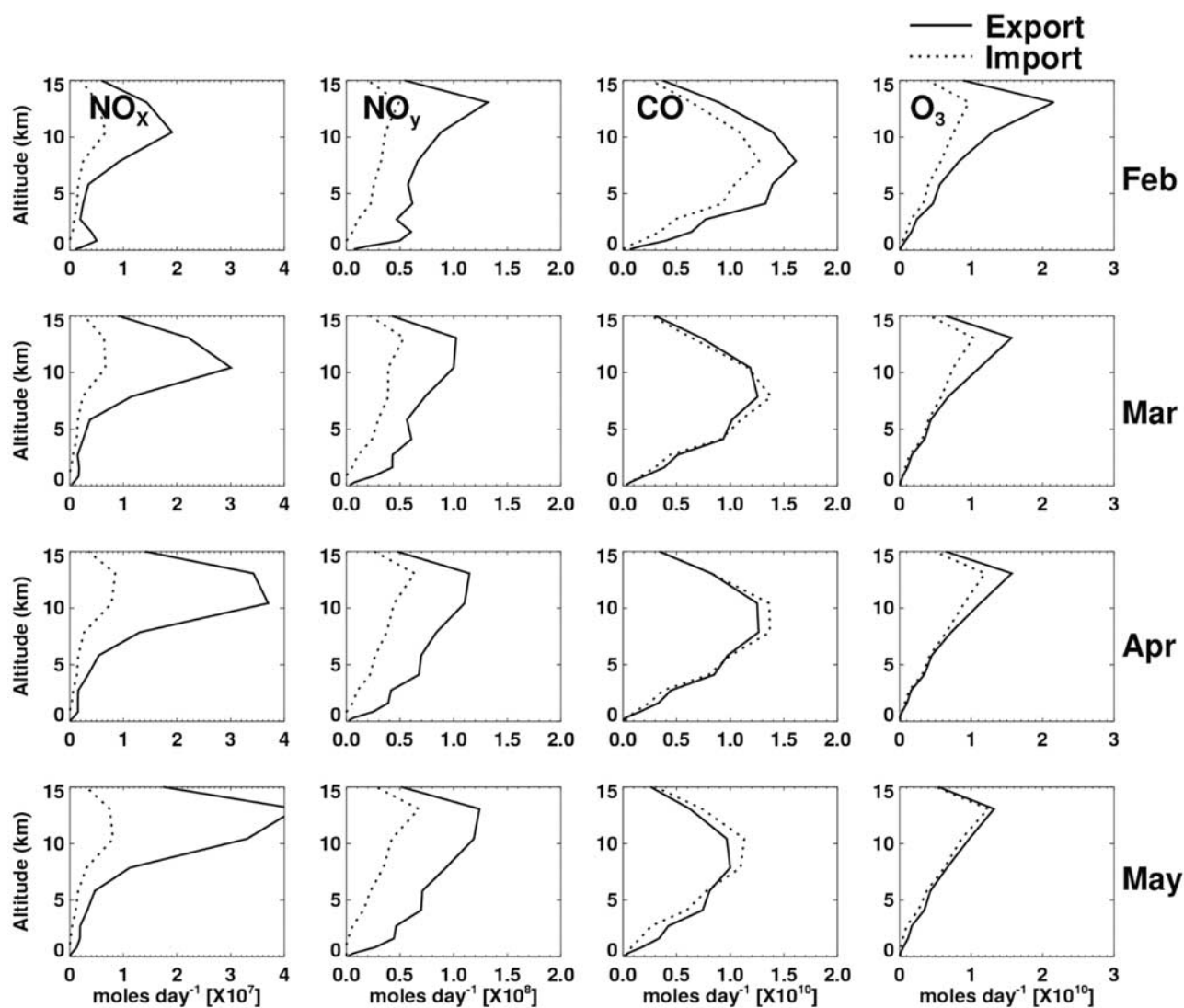


**Figure 10.** Vertical profiles of longitudinal import and export fluxes of  $\text{NO}_x$ ,  $\text{NO}_y$ ,  $\text{CO}$ , and  $\text{O}_3$  over North America in the troposphere. The western and eastern boundaries are the same as those depicted in Figure 9. The solid lines represent export fluxes while the dotted lines represent import fluxes.

difference between the two models is 3–20%, in the range of the standard deviation of monthly emission estimates (16–19%) for each model. These differences are averaged out during the 4-month period, leading to close agreement between a priori and top-down emission estimates.

[48] Measurements of tropospheric  $\text{NO}_x$  and  $\text{O}_3$  show clear seasonal changes and these changes are captured by REAM simulations. Over the continent, surface  $\text{NO}_x$  and tropospheric column  $\text{NO}_2$  decrease despite increasing lightning and soil emissions. Loss by photochemical oxidation of  $\text{NO}_x$  is larger than the source increase. In contrast, tropospheric column  $\text{NO}_2$  increases over the western North Atlantic. The increasing trend appears to be due to lightning  $\text{NO}$  emissions based on REAM results. Monthly mean lightning enhancements are  $0.5\text{--}2 \times 10^{15}$  and  $0.5\text{--}1.0 \times 10^{15}$  molecules  $\text{cm}^{-2}$  over the continent and western Atlantic, respectively. Some  $\text{NO}_x$  enhancements in May due to lightning and soil emissions are larger than GOME retrieval uncertainties, suggesting that satellite measurements may be used to constrain these emissions.

[49] Surface  $\text{O}_3$  over North America increases during spring as photochemistry activates. REAM performs well in simulating the multiday variations and seasonal transition. In comparison, the rate of surface  $\text{O}_3$  increase over the eastern United States in GEOS-CHEM is larger than in REAM (or AIRNow surface observations). A key factor driving the model difference is daytime mixing depth, which is much lower in REAM (simulated by MM5) than

**Table 2.** Import and Export Fluxes of Pollutants in the Boundary Layer (<2.5 km) Over North America (20–62°N)<sup>a</sup>

	Import Fluxes				Export Fluxes			
	Feb	Mar	Apr	May	Feb	Mar	Apr	May
$\text{NO}_x$	$<10^{-4}$	$<10^{-4}$	$<10^{-4}$	$<10^{-4}$	0.02	0.01	0.01	0.01
$\text{NO}_y$	0.01	0.02	0.02	0.01	0.31	0.20	0.19	0.21
$\text{CO}$	18	17	13	9	33	19	14	16
$\text{O}_3$	5.2	4.5	3.8	2.5	8.2	5.2	4.2	5.3

<sup>a</sup>Fluxes are measured in  $\text{Gmol d}^{-1}$ .

it is in GEOS-CHEM (simulated by GEOS-3). With limited supplies of radicals in the springtime, a larger daytime mixing depth in GEOS-CHEM results in faster photochemical activation because radical loss by the reaction of OH and NO<sub>2</sub> is less.

[50] In the free troposphere (400–800 hPa), ozonesonde and MOZAIC measurements show an increase of ~10 ppbv of O<sub>3</sub> from February to May. This increase is well simulated by REAM. Tropospheric O<sub>3</sub> columns derived from TOMS-SAGE II indicate significant increase over the western North Atlantic. Qualitative agreement is found in REAM results, although the simulated magnitudes are lower. Lightning NO<sub>x</sub> production is found to be the main contributor to the increase of column O<sub>3</sub> over the western North Atlantic.

[51] REAM model simulations are applied to investigate the pollutant imports and exports during spring. Lightning NO<sub>x</sub> production is a major contributor to the seasonal increase in the exports of NO<sub>x</sub> and NO<sub>y</sub> from North America in the upper troposphere. Simulated NO<sub>x</sub> export fluxes at 12 km increase by more than a factor of 2 from February to May (1.8 to 4 × 10<sup>7</sup> moles d<sup>-1</sup>). In May, lightning production enhances NO<sub>x</sub> and NO<sub>y</sub> exports in the upper troposphere (8–12 km) by 252% and 66%, respectively. In the boundary layer, the import fluxes of O<sub>3</sub> and CO consistently decrease, reflecting a decrease of long-range transport from spring to summer. The export fluxes of O<sub>3</sub>, CO, and NO<sub>x</sub> from the boundary layer do not exhibit large changes from March to May. The export efficiencies of NO<sub>x</sub> and NO<sub>y</sub> from the boundary layer are 0.6–0.7% and 12–14%, respectively.

## Appendix A

[52] The MOPITT instrument on board the NASA Terra satellite is capable of globally CO monitoring through observations in the thermal band around 4.6 μm. The satellite passes over the equator at around 1045 and 2245 local time, and the horizontal resolution of MOPITT is 22 × 22 km<sup>2</sup>. During March 2000, the first month when MOPITT data were collected, large amounts of data are missing due to calibrations. We compared REAM results to MOPITT for April and May 2000 (not shown). After processing the model results with the MOPITT averaging kernel [Deeter et al., 2003] and considering only the measurements with a priori portion <60%, we found that the correlation coefficients between simulated and MOPITT monthly mean CO columns are ~0.9 and that the monthly mean bias is ~1%.

[53] **Acknowledgments.** We thank Daniel Jacob and Robert Yantosca for providing GEOS-CHEM model and data, Mian Chin for providing aerosol optical depth data, Dale Allen and Louisa Emmons for helping us analyze MOPITT CO and ozonesonde data, and Kenneth Cummins for providing the NLDN effective detection efficiency. The GEOS-CHEM model is managed at Harvard University with support from the NASA Atmospheric Chemistry Modeling and Analysis Program. This work was supported by the National Science Foundation Atmospheric Chemistry Program.

## References

- Allen, D. J., J. E. Dibb, B. Ridley, K. E. Pickering, and R. W. Talbot (2003), An estimate of the stratospheric contribution to springtime tropospheric ozone maxima using TOPSE measurements and beryllium-7 simulations, *J. Geophys. Res.*, *108*(D4), 8355, doi:10.1029/2001JD001428.
- Atlas, E. L., B. A. Ridley, and C. Cantrell (2003), The Tropospheric Ozone Production about the Spring Equinox (TOPSE) Experiment: Introduction, *J. Geophys. Res.*, *108*(D4), 8353, doi:10.1029/2002JD003172.
- Bertram, T. H., et al. (2005), Satellite measurements of daily variations in soil NO<sub>x</sub> emissions, *Geophys. Res. Lett.*, *32*, L24812, doi:10.1029/2005GL024640.
- Bey, I. D., et al. (2001), Global modeling of tropospheric chemistry with assimilated meteorology: Model description and evaluation, *J. Geophys. Res.*, *106*, 23,073–23,096, doi:10.1029/2001JD000807.
- Black, T. L. (1994), The new NMC mesoscale ETA model: Description and forecast examples, *Weather Forecast.*, *9*, 265–278, doi:10.1175/1520-0434(1994)009<0265:TNNMEM>2.0.CO;2.
- Cantrell, C. A., et al. (2003), Steady state free radical budgets and ozone photochemistry during TOPSE, *J. Geophys. Res.*, *108*(D4), 8361, doi:10.1029/2002JD002198.
- Chance, K., et al. (2000), Satellite observations of formaldehyde over North America from GOME, *Geophys. Res. Lett.*, *27*, 3461–3464, doi:10.1029/2000GL011857.
- Chin, M., et al. (2002), Tropospheric aerosol optical thickness from the GOCART model and comparisons with satellite and sunphotometer measurements, *J. Atmos. Sci.*, *59*, 461–483, doi:10.1175/1520-0469(2002)059<0461:TAOTFT>2.0.CO;2.
- Choi, Y., Y. Wang, T. Zeng, R. Martin, T. Kurosu, and K. Chance (2005), Evidence of lightning NO<sub>x</sub> and convective transport of pollutants in satellite observations over North America, *Geophys. Res. Lett.*, *32*, L02805, doi:10.1029/2004GL021436.
- Deeter, M. N., et al. (2003), Operational carbon monoxide retrieval algorithm and selected results for the MOPITT instrument, *J. Geophys. Res.*, *108*(D14), 4399, doi:10.1029/2002JD003186.
- Emmons, L. K., et al. (2003), Budget of tropospheric ozone during TOPSE from two chemical transport models, *J. Geophys. Res.*, *108*(D8), 8372, doi:10.1029/2002JD002665.
- Fox-Rabinovitz, M. S., L. L. Takacs, and R. C. Govindaraju (2002), A variable-resolution? stretched-grid general circulation model and data assimilation system with multiple areas of interest: Studying anomalous regional climate events of 1998, *J. Geophys. Res.*, *107*(D24), 4768, doi:10.1029/2002JD002177.
- Geleyn, J. F. (1981), Some diagnostics of the cloud/radiation interaction in the ECMWF forecast model, paper presented at Workshop on Radiation and Cloud-Radiation Interaction in Numerical Modeling, Eur. Cent. for Medium-Range Weather Forecasts, Reading, U. K.
- Grell, G. A. (1993), Prognostic evaluation of assumptions used by cumulus parameterizations, *Mon. Weather Rev.*, *121*, 764–787, doi:10.1175/1520-0493(1993)121<0764:PEOAUB>2.0.CO;2.
- Guillas, S., J. Bao, Y. Choi, and Y. Wang (2008), Downscaling of chemical transport ozone forecasts over Atlanta, *Atmos. Environ.*, *42*, 1338–1348.
- Herman, J. R., and E. A. Celarier (1997), Earth surface reflectivity climatology at 340–380 nm from TOMS data, *J. Geophys. Res.*, *102*, 28,003–28,011, doi:10.1029/97JD02074.
- Holzworth, G. C. (1964), Estimates of mean maximum mixing depths in the contiguous United States, *Mon. Weather Rev.*, *92*, 235–242, doi:10.1175/1520-0493(1964)092<0235:EOMMMD>2.3.CO;2.
- Holzworth, G. C. (1967), Mixing Depths, Wind Speeds and Air Pollution Potential for Selected Locations in the United States, *J. Appl. Meteorol.*, *6*, 1039–1044, doi:10.1175/1520-0450(1967)006<1039:MDWSAA>2.0.CO;2.
- Horowitz, L. W., et al. (1998), Export of reactive nitrogen from North America during summertime: Sensitivity to hydrocarbon chemistry, *J. Geophys. Res.*, *103*, 13,451–13,476, doi:10.1029/97JD03142.
- Jing, P., et al. (2004), Isentropic cross-tropopause ozone transport in the Northern Hemisphere, *J. Atmos. Sci.*, *61*, 1068–1078, doi:10.1175/1520-0469(2004)061<1068:ICOTIT>2.0.CO;2.
- Jing, P., D. Cunnold, Y. Choi, and Y. Wang (2006), Summertime tropospheric ozone columns from Aura OMI-MLS measurements versus regional model results over the United States, *Geophys. Res. Lett.*, *33*, L17817, doi:10.1029/2006GL026473.
- Komhyr, W. D., et al. (1995), Electrochemical concentration cell ozonesonde performance evaluating during STOIC 1989, *J. Geophys. Res.*, *100*, 9231–9244, doi:10.1029/94JD02175.
- Kondo, Y., et al. (2004), Photochemistry of ozone over the western Pacific from winter to spring, *J. Geophys. Res.*, *109*, D23S02, doi:10.1029/2004JD004871.
- Kurosu, T. P., et al. (1999), CRAG: Cloud Retrieval Algorithm for the European Space Agency's Global Ozone Monitoring Experiment, paper presented at European Symposium of Atmospheric Measurements From Space, Eur. Space Agency, Paris.
- Lamarque, J.-F., and P. G. Hess (2003), Model analysis of the temporal and geographical origin of the CO distribution during the TOPSE campaign, *J. Geophys. Res.*, *108*(D4), 8354, doi:10.1029/2002JD002077.

- Liang, J., et al. (1998), Seasonal budgets of reactive nitrogen species and ozone over the United States, and export fluxes to the global atmosphere, *J. Geophys. Res.*, *103*, 13,435–13,450, doi:10.1029/97JD03126.
- Marenco, A., et al. (1998), Measurement of ozone and water vapor by Airbus in-service aircraft: The MOZAIC airborne program, An overview, *J. Geophys. Res.*, *103*, 25,631–25,642, doi:10.1029/98JD00977.
- Martin, R. V., et al. (1998), An improved retrieval of tropospheric nitrogen dioxide from GOME, *J. Geophys. Res.*, *107*(D20), 4437, doi:10.1029/2001JD001027.
- Martin, R. V., et al. (2003), Global inventory of nitrogen oxide emissions constrained by space-based observations of NO<sub>2</sub> columns, *J. Geophys. Res.*, *108*(D17), 4537, doi:10.1029/2003JD003453.
- National Research Council (1991), *Rethinking the Ozone Problem in Urban and Regional Air Pollution*, Natl. Acad. Press, Washington, D. C.
- Park, R. J., et al. (2004), Global simulation of tropospheric ozone using the Univ. of Maryland Chemical Transport Model (UMD-CTM): 2. Regional transport and chemistry over the central United States using a stretched grid, *J. Geophys. Res.*, *109*, D09303, doi:10.1029/2003JD004269.
- Price, C. (2000), Evidence for a link between global lightning activity and upper tropospheric water vapor, *Nature*, *406*, 290–293, doi:10.1038/35018543.
- Price, C., and D. Rind (1994), Modeling global lightning distributions in a general circulation model, *Mon. Weather Rev.*, *122*, 1930–1939, doi:10.1175/1520-0493(1994)122<1930:MGLDIA>2.0.CO;2.
- Price, C., et al. (1997), NO<sub>x</sub> from lightning 1. Global distribution based on lightning physics, *J. Geophys. Res.*, *102*(D5), 5929–5941, doi:10.1029/96JD03504.
- Rind, D. (1998), Just add water vapor, *Science*, *281*, 1152–1153, doi:10.1126/science.281.5380.1152.
- Spurr, R. J. D., et al. (2001), A linearized discrete ordinate radiative transfer model for atmospheric remote sensing retrieval, *J. Quant. Spectrosc. Radiat. Transfer*, *68*, 689–735, doi:10.1016/S0022-4073(00)00055-8.
- Stauffer, D. R., et al. (1991), Use of four-dimensional data assimilation in a limited-area mesoscale model part II. Effects of data assimilation within the planetary boundary layer, *Mon. Weather Rev.*, *119*, 734–754, doi:10.1175/1520-0493(1991)119<0734:UOFDDA>2.0.CO;2.
- Stephens, G., et al. (1978), Radiation profiles in extended water cloud III: Observations, *J. Atmos. Sci.*, *35*, 2133–2141, doi:10.1175/1520-0469(1978)035<2133:RPIEWC>2.0.CO;2.
- Thouret, V., et al. (1998), Ozone climatologies at 9–12 km altitude as seen by the MOZAIC airborne program between September 1994 and August 1996, *J. Geophys. Res.*, *103*, 25,653–25,679, doi:10.1029/98JD01807.
- Thouret, V., et al. (2006), Tropopause referenced ozone climatology and inter-annual variability (1994–2003) from the MOZAIC programme, *Atmos. Chem. Phys.*, *6*, 1033–1051.
- U. S. Environmental Protection Agency (2003), National air quality and emissions trends report, 1980, 1985, 1989–2000, Research Triangle Park, N. C.
- Walcek, C. J. (2000), Minor flux adjustment near mixing ratio extremes for simplified yet highly accurate monotonic calculation of tracer advection, *J. Geophys. Res.*, *05*, 9335–9348, doi:10.1029/1999JD901142.
- Wang, H.-J., et al. (2002), Assessment of SAGE version 6.1 ozone data quality, *J. Geophys. Res.*, *107*(D23), 4691, doi:10.1029/2002JD002418.
- Wang, H.-J., et al. (2006), SAGE III solar ozone measurements: Initial results, *Geophys. Res. Lett.*, *33*, L03805, doi:10.1029/2005GL025099.
- Wang, Y., et al. (1998), Global simulation of tropospheric O<sub>3</sub>-NO<sub>x</sub>-hydrocarbon chemistry: 1. Model formulation, *J. Geophys. Res.*, *103*, 10,713–10,725, doi:10.1029/98JD00158.
- Wang, Y., et al. (2003a), Springtime photochemistry at northern mid and high latitudes, *J. Geophys. Res.*, *108*(D4), 8358, doi:10.1029/2002JD002227.
- Wang, Y., et al. (2003b), Intercontinental transport of pollution manifested in the variability and seasonal trend of springtime O<sub>3</sub> at northern mid and high latitudes, *J. Geophys. Res.*, *108*(D21), 4683, doi:10.1029/2003JD003592.
- Wang, Y., Y. Choi, T. Zeng, B. Ridley, N. Blake, D. Blake, and F. Flocke (2006), Late-spring increase of trans-Pacific pollution transport in the upper troposphere, *Geophys. Res. Lett.*, *33*, L01811, doi:10.1029/2005GL024975.
- Wang, Y., Y. Choi, T. Zeng, D. Davis, M. Buhr, G. Huey, and W. Neff (2007), Assessing the photochemical impact of snow NO<sub>x</sub> emissions over Antarctica during ANTCI 2003, *Atmos. Environ.*, *41*, 3944–3958, doi:10.1016/j.atmosenv.2007.01.056.
- Yienger, J. J., and H. Levy II (1995), Empirical model of global soil-biogenic NO<sub>x</sub> emissions, *J. Geophys. Res.*, *100*, 11,447–11,464, doi:10.1029/95JD00370.
- Zeng, T., et al. (2003), Widespread persistent near-surface ozone depletion at northern high latitudes in spring, *Geophys. Res. Lett.*, *30*(24), 2298, doi:10.1029/2003GL018587.
- Zeng, T., et al. (2006), Halogen-driven low altitude O<sub>3</sub> and hydrocarbon losses in spring at northern high latitudes, *J. Geophys. Res.*, *111*, D17313, doi:10.1029/2005JD006706.

K. Chance, Harvard-Smithsonian Center for Astrophysics, 60 Garden Street, Cambridge, MA 02138-1516, USA.

Y. Choi, Jet Propulsion Laboratory, California Institute of Technology, Pasadena, CA 91109, USA.

D. Cunnold, Y. Wang, E.-S. Yang, and T. Zeng, School of Earth and Atmospheric Sciences, Georgia Institute of Technology, Atlanta, GA 30332-0340, USA. (ywang@eas.gatech.edu)

E. Edgerton, Atmospheric Research and Analysis, Inc., 3500 Cottonwood Drive, Durham, NC 27707, USA.

R. Martin, Department of Physics and Atmospheric Science, Dalhousie University, Halifax, NS B3H 3J5, Canada.

V. Thouret, Laboratoire d'Aerologie, CNRS, 14 avenue Edouard Belin, F-31400 Toulouse, France.